

NUMERICAL ALGORITHMS AND MESH DEPENDENCE IN THE DISTURBED STATE CONCEPT

CHANDRA S. DESAI,^{1*†} CEMAL BASARAN^{2‡} AND WU ZHANG^{1§}

¹*Department of Civil Engineering and Engineering Mechanics, The University of Arizona, Tucson, Arizona, U.S.A.*

²*Department of Civil Engineering, State University of New York, Buffalo, New York, U.S.A.*

ABSTRACT

The disturbed state concept (DSC) provides a unified approach for constitutive modelling of engineering materials including such factors as elastic, plastic and creep strains, microcracking, damage and softening, and stiffening responses. The interacting mechanisms in the material mixture composed of the relative intact and fully adjusted states provide implicitly for various factors such as microcrack interaction and characteristic dimension. The DSC model can allow for well-posedness, reduction or elimination of spurious mesh dependence and localization. A number of problems are solved to illustrate convergence and uniqueness of the finite element procedures, localization, spurious mesh dependence, and validation with respect to observed behavior of simulated and practical problems. © 1997 by John Wiley & Sons, Ltd.

Int. J. Numer. Meth. Engng., **40**, 3059–3083 (1997)

No. of Figures: 16. No. of Tables: 0. No. of References: 39.

KEY WORDS: disturbed state concept; softening; finite element algorithms; localization; mesh dependence; validations

INTRODUCTION

It is well known that a computational (e.g. finite element) procedure based on the traditional continuum theory exhibits spurious or pathological mesh sensitivity when it is used to represent the behaviour of materials that experience discontinuous and non-homogeneous conditions due to microcracking, damage and softening.^{1–5} In the traditional finite element procedure, based on the continuum theory in which strains and stresses are defined at a point, the influence of microcracking in tributary neighbouring zones is not included in the behaviour. As a result, when such discontinuities occur, they may be restricted within a single finite element zone. It is reported^{4,6} that as the element or damage zone becomes smaller, the energy required to propagate the crack or damage tends to zero. This would indicate that the material could fail at

* Correspondence to: C. S. Desai, Department of Civil Engineering and Engineering Mechanics, The University of Arizona, Tucson, AZ 85721-0072, U.S.A.

† Regents' Professor

‡ Assistant Professor

§ Graduate Student

Contract grant sponsor: National Science Foundation; Contract grant numbers: DDM-9102177, DDM-9313204

zero-energy dissipation, which is physically unrealistic, and as a consequence, the cracks (or strains) localize into a single element wide zone.

To reduce or eliminate the foregoing localization phenomenon, several models are proposed that often constitute enrichment or enhancement of the continuum models.^{2,5,7-11} These models include the *non-local* formulation proposed by Eringen¹² and Kroner¹³ and developed extensively further by Bazant and coworkers.⁴ De Borst *et al.*⁵ have presented a comprehensive review and analysis of these enrichment models, which include the gradient theory, micropolar models, fracture energy and Cosserat continuum approaches.

In this paper, an alternative and unified approach called the *disturbed state concept* (DSC) is proposed for modelling the mechanical behaviour of materials and interfaces, including effects such as elastic, plastic and creep strains, volume changes, stress paths, microcracking, damage and softening and strengthening responses.¹⁴⁻²⁰

The DSC model allows for relative motions (translation and rotation) between material clusters that constitute the mixture of material parts in the relative intact (RI) and fully adjusted (FA) states, which are defined later. Together with a simple averaging scheme for strains, the DSC allows for non-local effects, localization limiter and size effects. As a result, in general, the DSC can reduce or eliminate the spurious mesh dependence: however, for the problems considered herein such an effect is essentially eliminated. This paper contains the following major items:

- (1) a brief review of the previous non-local and enrichment models,
- (2) a brief description of the DSC,
- (3) analysis of the DSC regarding relative motions, ellipticity, localization limiter, size effect and tangent stiffness matrix,
- (4) implementation of the DSC in computational (finite element) procedure, and
- (5) examples of validation of the DSC involving spurious mesh dependence, finite element analysis of a concrete tested in the laboratory, localization in a one-dimensional bar with imperfection, and localization of disturbance in a chip-substrate problem in electronic packaging under cyclic thermal loading.

REVIEW

Among the damage, non-local damage and the latter with microcrack interaction models, reference is made to works of Kachanov,^{21,22} Lemaitre and Chaboche,²³ Bazant and coworkers,^{4,24} Krajcinovic and coworkers,²⁵ Schreyer and coworkers,^{1,26} Mühlhaus, de Borst and Aifantis^{5,10,11,27} have proposed and developed enrichments models based on gradient, micropolar and Cosserat theories; de Borst *et al.*⁵ have presented a comprehensive overview and analysis related to the loss of ellipticity, well-posedness, positive definiteness, localization and spurious mesh sensitivity for these models.

Non-local considerations

In a philosophical sense, non-locality can be explained as the necessity that the behaviour at a point in a material system include the effect of the behaviour of neighbouring zones, consistent with the material's interlinkedness that pervades all physical systems. In other words, microcracking and damage (at a point) should include interacting influences from points in the tributary zones, often beyond the nearby and adjacent zones. In the case of the finite element analysis,

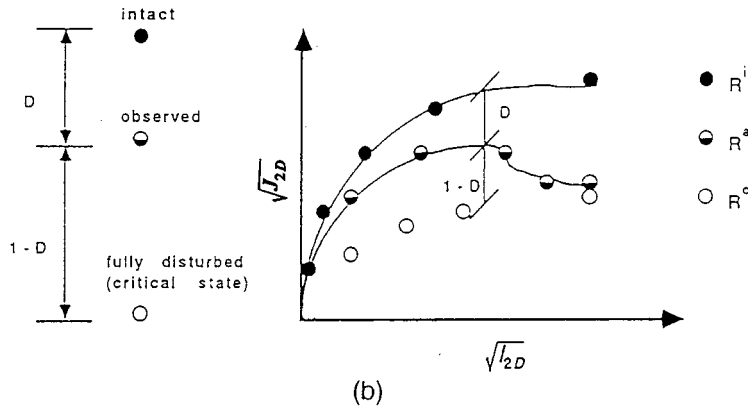
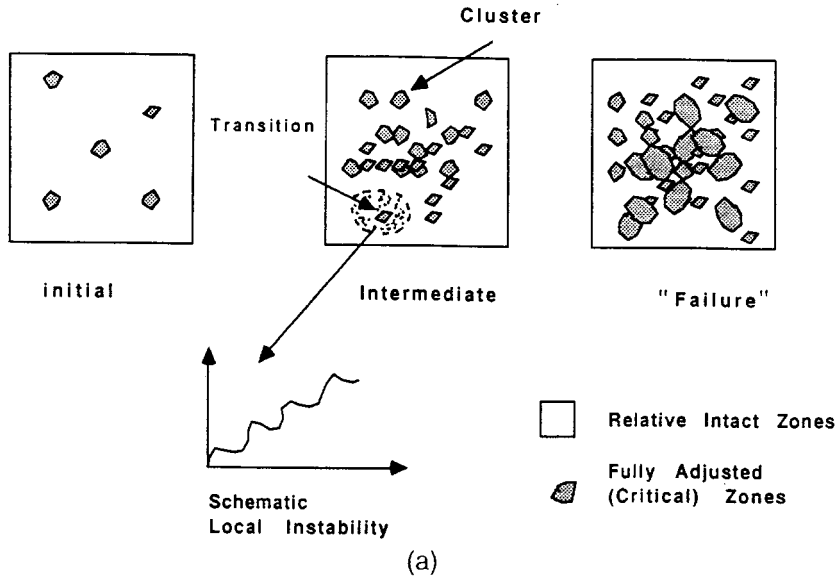


Figure 1. Representation of disturbed state concept ($R \Rightarrow$ response): (a) schematic of relative intact and fully adjusted clusters in DSC; (b) schematic of disturbed state concept

microcracking and damage in an element should allow for the influence of the response of tributary zones that include elements beyond those involved in the direct stiffness assembly governed by the approximation functions adopted. If such effects are not included, the patterns and the extent of the clusters involving microcracking (Figure 1(a)) will be dependent on the given mesh, leading to the spurious mesh sensitivity problem.

Thus, in the non-local approach, the basic idea is that the influence of microcracking and damage in the neighbouring zone, should be included in the definition of strains and other

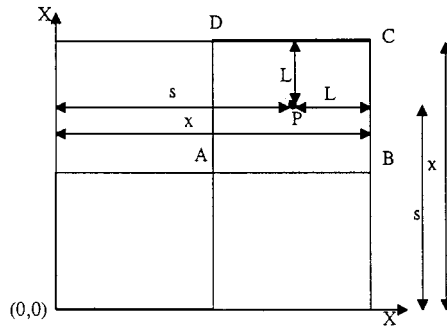


Figure 2. Nonlocal continuum averaging procedure

quantities. For example, the non-local or average strain $\tilde{\varepsilon}(x)$ is then expressed as⁴

$$\tilde{\varepsilon}(x) = \frac{\int_V W(x - s) \varepsilon(s) dV(s)}{\int_V W(x - s) dV(s)} \tag{1}$$

where $\varepsilon(s)$ is the local strain at a point in the tributary zone (area) of point s (e.g. a Gauss integration point in the finite element analysis), W is the weight function for point P , V is the volume, x is shown in Figure 2, and the accent over ε denotes spatial averaging. A simplified averaging procedure is used with the DSC and is described later.

DISTURBED STATE CONCEPT

Details of the disturbed state concept (DSC), including a comparison with classical damage, non-local damage with microcrack interaction, micromechanics and self-organized criticality (SOC),²⁸ have been presented by Desai¹⁵ and Desai and Toth.²⁰ Here, only a brief description is given.

In the DSC, it is assumed that applied mechanical and environmental forces cause disturbances or changes in the material’s microstructure with respect to its behaviour under its *relative intact* (RI) and *fully adjusted* (FA) states. The RI state refers to the behaviour of the material that excludes the influences of factors such as friction, anisotropy, microcracking, damage, softening and stiffening or growth.¹⁵ In the RI state, the material is modelled by using a continuum theory. The FA state refers to the asymptotic (‘equilibrium’) state to which the material tends to in the ultimate stages of deformation. The material in the RI state is transformed continuously into the FA state through a process of natural *self-adjustment* of its microstructure.

At any stage during deformation the material is treated as the mixture of the RI and FA parts, which are distributed (randomly) over the material elements (Figure 1(a)). The RI and FA states of the material are called the *reference* states. The material is initially in a full or a partial RI state, depending upon the *initial* disturbance, due to factors such as initial stresses, anisotropy and manufacturing. During the deformation, the volume of the material in the FA state increases, and the volume of the RI state material decreases. This process involves continuous interaction between the material parts in the RI and FA states.

The observed response of the mixture is expressed in terms of the responses of the material in the RI and FA states by using the disturbance function, which denotes deviation of the observed behaviour from those of the two reference states; a symbolic representation is shown in Figure 1(b). Here, J_{2D} and I_{2D} are the second invariants of the deviatoric stress and strain tensors, respectively.

The behaviour of the material in the RI state can be simulated by using a theory based on continuum mechanics, such as linear or non-linear elasticity, elastoplasticity, viscoplasticity or thermoviscoplasticity.^{15,18–20} The FA state can be represented as (1) the ‘failed’ material which acts like a ‘void’ as in the classical damage theory^{21,22} and can carry no stress at all, (2) it can carry hydrostatic stress but no shear stress, like a *constrained liquid*^{15,29} or (3) it can continue to carry the shear stress for a given hydrostatic stress, reached up to that point and can deform under constant volume, as in the case of the critical state soil mechanics concept;^{15,30} here, the material acts like a *constrained liquid–solid*. As the FA material is constrained by the surrounding RI material, the two latter simulations are considered to be more realistic than the first one. At this time, as the disturbance, D , is assumed to be a scalar, the FA response is not influenced by stress paths.

Consequently, the DSC includes the coupled (observed) response, as it is influenced by the *collective behaviour of the interacting mechanisms* in the RI and FA states. Hence, the material response is represented in a unified manner based upon the observed responses of the material in the RI and FA states. Thus, it is not necessary to measure and define particle level constitutive response, as in the case of micromechanics models. Also, since the microcrack interaction is included implicitly in the model, it is not necessary to superimpose effects of forces and kinematics in individual or collected microcracks with the damage theory.²⁴

GOVERNING EQUATIONS

Based on the equilibrium of forces in the observed (mixture), RI and FA states, the incremental observed stress tensor, $d\sigma_{ij}^a$, is derived as^{15,20}

$$d\sigma_{ij}^a = (1 - D)d\sigma_{ij}^i + Dd\sigma_{ij}^b + dD(\sigma_{ij}^c - \sigma_{ij}^i) \tag{2a}$$

in which

$$\sigma_{ij}^a = (1 - D)\sigma_{ij}^i + D\sigma_{ij}^c, \tag{2b}$$

and where a, i and c denote observed, RI and FA states, respectively, D is the scalar disturbance function (described later), and d denotes increment. In Equation (2a), $\sigma_{ij}^r = \sigma_{ij}^c - \sigma_{ij}^i$ denotes the relative stress as the difference between the stresses in the FA and RI states; Figure 3 shows a symbolic representation in which the randomly distributed clusters in the RI and FA states are collected in a weighted sense. Equations (2a) can be written as

$$d\sigma_{ij}^a = (1 - D)C_{ijkl}^i d\epsilon_{kl}^i + DC_{ijkl}^c d\epsilon_{kl}^c + dD\sigma_{ij}^r \tag{3}$$

where C_{ijkl} is the fourth-order tensor related to the constitutive behaviour.

In the DSC, the relative stress (σ_{ij}^r) can cause relative motions (translation, rotations). Together with the second term on the right-hand side in equation (3), they incorporate the effect of microcrack interaction. As a consequence of the relative stress, σ_{ij}^r , the strains, $d\epsilon_{ij}$, are different in

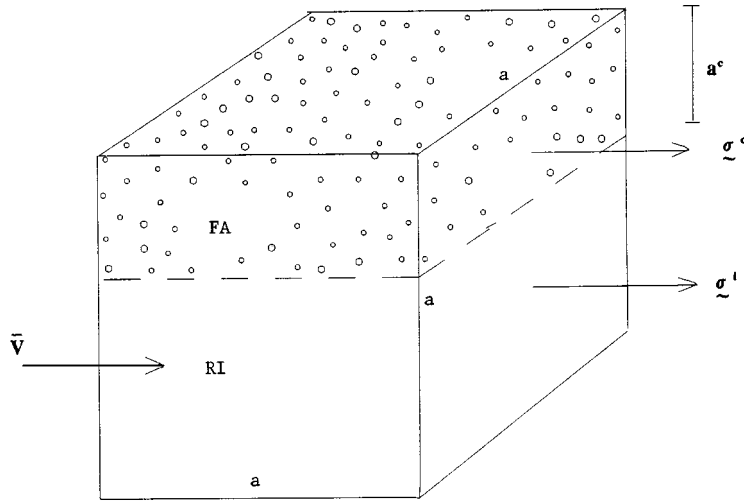


Figure 3. Stresses in RI and FA parts and relative motion

the FA and RI states. Thus, ϵ_{ij}^i and ϵ_{ij}^e are the tensors of strains in the RI and FA parts, respectively. It is usually difficult to establish a relationship between these two strains; in the finite element analysis, it is evaluated during the incremental loading through the iterative procedure starting from the assumption that they are initially equal. A simple relation between the two can be expressed as¹⁹

$$d\epsilon_{ij}^e = (1 + \alpha)d\epsilon_{ij}^i \tag{4}$$

where α is the relative motion parameter, which can be the function of deformation history, e.g. plastic strain trajectory and the disturbance. Also, dD can be derived as¹⁹

$$dD = R_{ij}d\epsilon_{ij}^i \tag{5a}$$

where, with the plasticity model and disturbance D (described later), R_{ij} is given by

$$R_{ij} = \frac{(D_u AZ \xi_D^z - 1 e^{-A\xi_D^z}) \frac{\partial F}{\partial \sigma_{uv}} C_{uvst}^e \left(\frac{\partial F}{\partial \sigma_{ij}} \frac{\partial F}{\partial \sigma_{ij}} - \frac{1}{3} \frac{\partial F}{\partial \sigma_{ii}} \frac{\partial F}{\partial \sigma_{ii}} \right)^{1/2}}{\frac{\partial F}{\partial \sigma_{mn}} C_{mnpq}^e \frac{\partial F}{\partial \sigma_{pq}} - \frac{\partial F}{\partial \xi} \left(\frac{\partial F}{\partial \sigma_{mn}} \frac{\partial F}{\partial \sigma_{mn}} \right)^{1/2}} \tag{5b}$$

D_u , A and Z are parameters in D , see later equation (8), ξ and ξ_D are the trajectories of plastic total and deviatoric strains, respectively, F is the yield function and superscript e denotes elastic.

Then, equation (3) can be rewritten as

$$d\sigma_{ij}^a = [(1 - D)C_{ijkl}^i + D(1 + \alpha)C_{ijkl}^e + \sigma_{ij}^r R_{kl}] d\epsilon_{kl}^i \tag{6a}$$

$$d\sigma_{ij}^a = (L_{ijkl} + L_{ijkl}^r) d\epsilon_{kl}^i \tag{6b}$$

or

$$d\sigma_{ij}^a = \bar{C}_{ijkl} de_{kl}^i \tag{6c}$$

where

$$L_{ijkl} = (1 - D) C_{ijkl}^i + D(1 + \alpha) C_{ijkl}^c$$

and

$$L_{ijkl}^r = \sigma_{ij}^r R_{kl}$$

Disturbance function

The disturbance which is caused by loading and which is influenced by the physical properties of the material is considered to denote the deviation of the observed behaviour with respect to the behaviour of the materials in the reference states. The disturbance function, D , can be defined based on observed stresses, volumetric response, and/or nondestructive (ultrasonic) velocities during loading, unloading and reloading; details are given elsewhere.²⁰ Here, D , based on stresses, is defined as (Figure 4)

$$D = \frac{\bar{\sigma}^i - \bar{\sigma}^a}{\bar{\sigma}^i - \bar{\sigma}^c} \tag{7}$$

where $\bar{\sigma}$ is the equivalent stress such as $\sqrt{J_{2D}}$, the second invariant of the deviatoric stress tensor, S_{ij} , or τ , the octahedral shear stress. At this time, it is assumed that the RI response is stiffer than the observed response; hence, D is positive. If it is softer than the observed response, D will be negative, indicating stiffening or strengthening in the observed response; such a behaviour can be

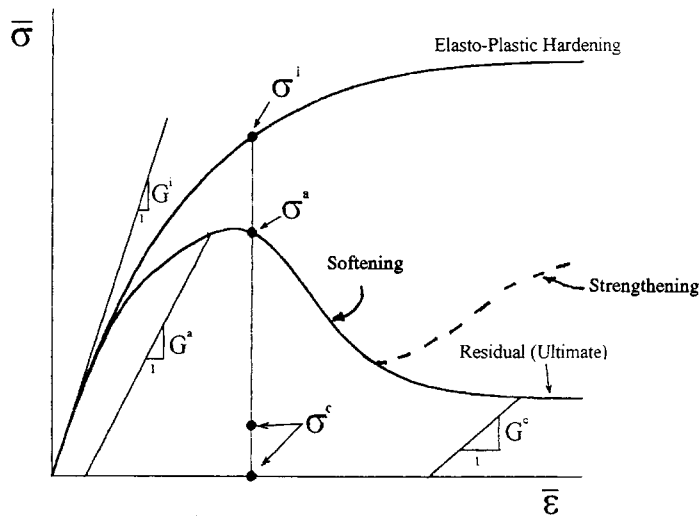


Figure 4. Schematic of stress–strain response and disturbance

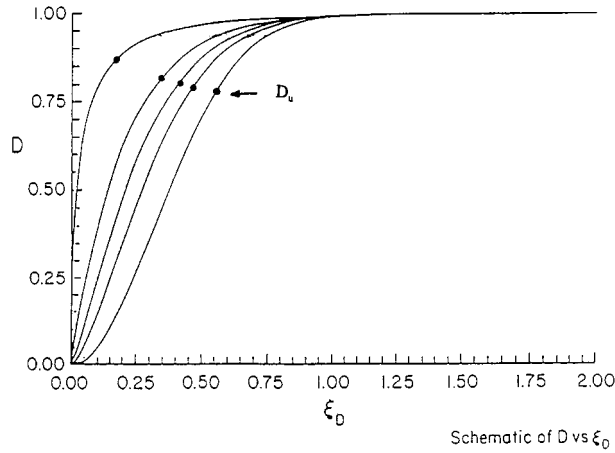


Figure 5. Schematic of disturbance function

included with additional analysis. Now, D is expressed as

$$D = D_u [1 - \exp(-A \zeta_D^Z)] \tag{8}$$

where A and Z are material parameters and D_u is the value of D corresponding to the residual condition (Figure 4). A schematic of D vs. ζ_D is shown in Figure 5; here, ζ_D is the trajectory of deviatoric plastic strains, E_{ij}^p , as

$$\zeta_D = \int (dE_{ij}^p dE_{ij}^p)^{1/2} \tag{9}$$

Here, ζ_D is based on irreversible or plastic strains corresponding to the observed response. However, as a simplification, it can be approximated in terms of plastic strains corresponding to the RI response based on the hierarchical (δ_0) plasticity model.³¹

Note that the form of the disturbance function is similar to the classical damage parameter, ω . Further comparisons and difference of D from the classical²¹ damage parameter are discussed by Desai¹⁵ and Desai and Toth.²⁰

ANALYSIS

The DSC with the relative motion between the FA and RI parts yields a diffusion-type process. Various characteristics of the model are discussed below.

Let the non-local or average strains $d\tilde{\epsilon}_{ij}$ be expressed by a simple form of equation (1) as

$$d\tilde{\epsilon}_{ij} = \frac{\int_V d\epsilon_{ij}^a dV}{\bar{V}} \tag{10}$$

where \bar{V} is the tributary volume. Following Mühlhaus *et al.*,²⁷ equation (10) can be written as

$$d\tilde{\varepsilon}(y_i) = \frac{1}{a^3} \int d\varepsilon_{ij}^a(y_i + s_i) ds_1 ds_2 ds_3 \tag{11}$$

where $\bar{V} = a^3$ (Figure 3), a is the dimension of the characteristic volume, $|s_i| \leq a/2$ and $s_i = x_i - y_i$. Now, $d\varepsilon_{ij}^a$ can be expressed using Taylor series as

$$d\varepsilon_{ij}^a(y_i + s_i) = d\varepsilon_{ij}^a(y_i) + \frac{1}{1!} \left(\frac{\partial(d\varepsilon_{ij}^a)}{\partial x_i} \right)_{x_i=y_i} s_i + \frac{1}{2!} \left(\frac{\partial^2(d\varepsilon_{ij}^a)}{\partial x_i \partial x_j} \right)_{x_i=y_i} s_i s_j + \dots \tag{12}$$

Substitution of equation (12) into equation (11) gives

$$d\tilde{\varepsilon}_{ij}(y_i) \simeq d\varepsilon_{ij}^a + \frac{a^2}{24} [\nabla^2(d\varepsilon_{ij}^a)]_{x_i=y_i} \tag{13}$$

where $\nabla^2(\cdot) = (\partial^2/\partial x_i \partial x_i)(\cdot)$ is the Laplace operator. Furthermore, equation (2a) can be expressed as

$$d\sigma_{ij}^a = d\sigma_{ij}^i + (Dd\sigma_{ij}^r + dD\sigma_{ij}^r) \tag{14a}$$

where $\sigma_{ij}^r = \sigma_{ij}^c - \sigma_{ij}^i$ and $d\sigma_{ij}^r = d\sigma_{ij}^c - d\sigma_{ij}^i$. Equation (14a) can be written as

$$d\sigma_{ij}^a = d\sigma_{ij}^i + g_{ij}(\tilde{\varepsilon}_{ij}^p, d\tilde{\varepsilon}_{ij}^p, a, da) \tag{14b}$$

where a and da are characteristic dimensions and its increment corresponding to the total (σ_{ij}^r) and incremental ($d\sigma_{ij}^r$) relative stresses, respectively. The form of incremental (or rate of) stress, equation (14b), can be considered similar to that in the gradient plasticity model.^{5,11}

Referring to Figure 3, the above relative stresses can be considered to introduce moments M_{ij} in the material element:

$$M_{ij} = \frac{a^c}{a} (\sigma_{ij}^c - \sigma_{ij}^i) \tag{15}$$

Here, a^c is the dimension that involves the FA or critical part, and $a^c/a = D$, the disturbance. The value of a^c is bounded by its ultimate (or residual) value, a_u^c , corresponding to the ultimate $D_u (< 1)$ in the residual state (Figure 4). Furthermore, the disturbance parameters, A , Z and D_u , can be functions of such factors as initial density, confining pressure and length scale. The length scale can be in terms of a characteristic dimension (related to the particle size), length to diameter ratio of test specimen or other suitable measure. For instance, consider disturbance, D_E , in a computer (finite element) procedure, and in a laboratory test, D_T , which can be related as

$$D_E = \left(\frac{V_T}{V_E} \right) \left(\frac{V_E^c}{V_T^c} \right) D_T \tag{16}$$

where V_E and V_T are the volumes of the finite element and laboratory test specimen, respectively. With the definition of D , equation (8), in the DSC, the disturbance is dependent on the dimensions (size) of the test specimen, e.g. expressed as the ratio of L/\bar{D} , where L is the length of the element and \bar{D} is the (mean) diameter. This is illustrated in Figure 6 which shows laboratory behaviour of cylindrical specimens with different values of L/\bar{D} for a soft (artificial) rock tested under uniaxial compression loading.³² Figure 6(b) shows that the disturbance D is dependent on the L/\bar{D} ratio. Thus, the disturbance, D , can include effects of the length scale and size, which can act to control

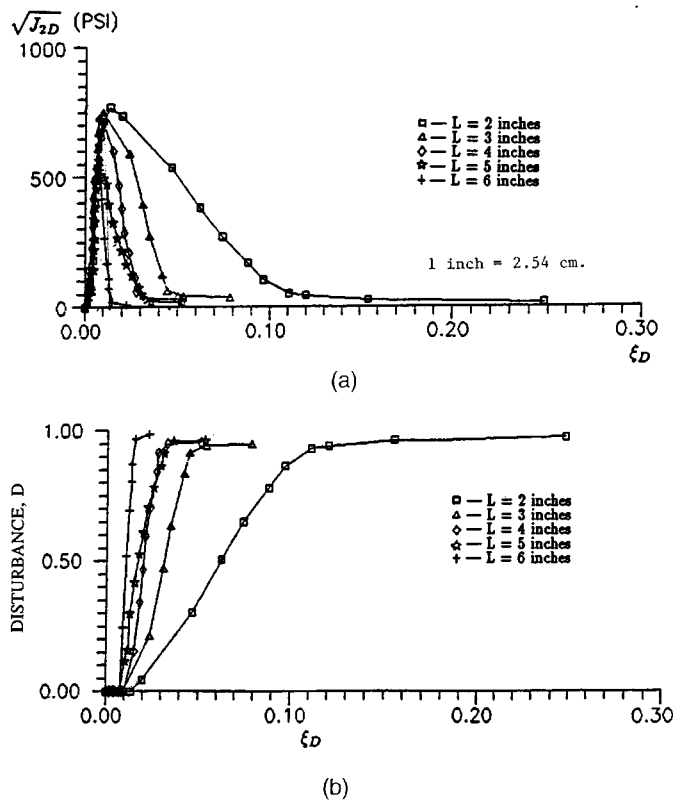


Figure 6. Stress-strain behavior of soft rock for different L/\bar{D} ratios: $\bar{D} = 3.0$ in: (a) $\sqrt{J_{2D}}$ vs. ξ_D ; (b) disturbance vs. ξ_D

localization. An example is given subsequently. It may be noted that the DSC model can often provide satisfactory solutions with averaging of strains only over an element, as it is commonly done in finite element analysis. However, improved results can be obtained by using the averaging over a patch of elements.

In view of the above, the DSC model is considered to include implicitly terms similar to those in gradient plasticity. As a result, it can guarantee ellipticity and well-posedness properties, and allow for localization limiter and regularization. Inclusion of the averaging procedure and the relative motion contribute towards elimination of spurious mesh dependence. The relative motion between the RI and FA parts caused by different stresses in the two parts introduce additional energy terms in the formulation and provides a stabilizing effect.

FINITE ELEMENT EQUATIONS

Based on the virtual work principle, the finite element equations corresponding to equation (6) are derived as¹⁹

$$\int_V ([B]^T [L] [B] + [B]^T [L^r] [B]) \{dq^i\} = \{Q\} - \int [B]^T \{\sigma^a\} dV \quad (17a)$$

or

$$\int_V ([B^T][\bar{C}][B]) dV \{dq^i\} = \{Q\} - \int_V [B]^T \{\sigma^a\} dV \tag{17b}$$

where $[B]$ is the strain–displacement transformation matrix in $\{d\varepsilon^i\} = [B]\{dq^i\}$, $\{q\}$ is the vector of nodal displacement, and $\{Q\}$ is the external load vector. Equation (17a) or (17b) involves two unknowns, $\{dq^i\}$, $\{\sigma^r\}$. The detailed solution scheme is given by Basaran and Desai¹⁹ and is briefly outlined below.

Solution schemes

Equations (17) can be solved using the following schemes:

- (1) Equations (17) are solved using an incremental iterative procedure under strain controlled condition. Here, the tangent matrix $[\bar{C}]$ is not positive definite, particularly in the strain-softening zone. However, with the strain-controlled loading, the procedure provides convergent and accurate solutions, which is illustrated below through solutions of a one-dimensional case, mesh-sensitivity analysis, comparison with laboratory test results for a concrete, one-dimensional bar with imperfection, and thermomechanical analysis of a chip-substrate problem in electronic packaging.
- (2) The term related to the relative stress, σ_{ij}^r is taken to the right-hand side, to lead to

$$\begin{aligned} \int_V ([B]^T [L][B] dV)_{n-1} \{dq^i\}_n = \{Q\}_n - \int_V [B]^T \{\sigma^a\}_{n-1} dV \\ - \int_V [B^T][L^r][R] dV \{dq^i\}_{n-1} \end{aligned} \tag{18}$$

Here, the term related to $[L^r]$ is evaluated as the load vector at the previous increment $n - 1$. Then, the system matrix on the left-hand side is always positive definite because $0 \leq D \leq D_u$, and $\alpha \geq 0$. Such a transformation does not change the positive- or negative-definite character of the problem; however, it can provide an approximate and simpler procedure for the finite element analysis. The algorithm in equation (18) is considered to be similar to those in the non-local damage models.^{4,7}

- (3) The term $\{\sigma^r\}$ can be treated as an independent (constraint) unknown, together with the displacements, and the problem is treated as coupled. This would lead to coupled equations as

$$\begin{bmatrix} K_{11} & K_{12} \\ K_{21} & K_{22} \end{bmatrix} \begin{Bmatrix} dq^i \\ d\sigma^r \end{Bmatrix} = \begin{Bmatrix} \bar{Q} \\ 0 \end{Bmatrix} \tag{19}$$

which are solved simultaneously for $\{dq^i\}$ and $\{d\sigma^r\}$. This procedure would be relatively more time-consuming than the first two; however, it can provide a more general solution in the sense that both the displacement and constraint are assumed unknowns, as in a mixed formulation, and are evaluated simultaneously. Equation (19) is similar to other formulations.^{11,33} It may be noted that the simplified equations (17) and (18) include the term corresponding to $\{d\sigma^r\}$ in equation (19).

Computation of stresses

Solution of equation (18) yields displacement increment for the RI state, $\{dq^i\}_n$ at step n . It is used to compute $\{d\varepsilon^i\}_n$ as

$$\{d\varepsilon^i\}_n = [B] \{dq^i\}_n \quad (20)$$

Then the RI stress increment is found as

$$\{d\sigma^i\}_n = [C]^i \{d\varepsilon^i\}_n \quad (21)$$

which leads to the evaluation of observed stress increment $\{d\sigma^a\}_n$

$$\{d\sigma^a\}_n = (1 - D_n) \{d\sigma^i\}_n + D_n \{d\sigma^c\}_n + (\{\sigma^c\}_n - \{\sigma^i\}_n) dD_n \quad (22)$$

The increment of stress in the FA material can be evaluated by using the critical state concept.¹⁵ Here, as a simplification, it is assumed that the FA part does not carry any shear stress, and the mean stresses and its increment in the RI and FA parts are equal. The total stresses $\{\sigma^i\}_n$ and $\{\sigma^c\}_n$ are obtained by accumulating the incremental stresses. The value of disturbance, D_n , is found using equation (8) based on computed trajectory of plastic strain increment, ξ_D . Then, dD_n is found as

$$dD_n = D_n - D_{n-1} \quad (23)$$

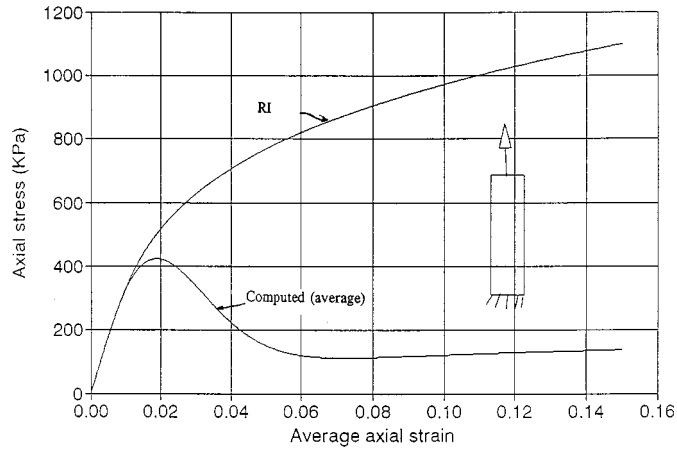
EVALUATION AND VERIFICATIONS

In order to verify the DSC, five examples are considered: (1) one-dimensional tension loading of a bar to illustrate properties of the tangent stiffness matrix, (2) unconfined block subjected to surface loading to illustrate mesh sensitivity, (3) comparisons of prediction with laboratory test for a cubical specimen, (4) localization in a one-dimensional bar with imperfection and (5) localization analysis of a chip-substrate problem under thermal loading. For the first three examples, the material considered is a concrete which was tested under strain-controlled and three-dimensional loading by Van Mier.³⁴ The material parameters for the concrete^{29,35} for the DSC model are shown in Appendix together with brief description of the plasticity model for the RI state.

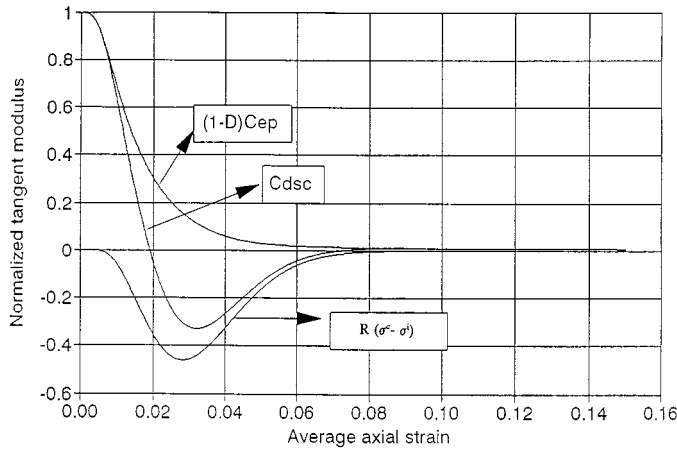
Tangent stiffness matrix

The one-dimensional bar element of size: 20 cm length, 10 cm width, and 1 cm thickness, is shown in Figure 7(a). It is subjected to incremental (tensile) displacements of 0.03 cm each step, with a total of 100 loading steps.

Figure 7(a) shows the RI (intact) and observed (average) behaviour obtained by using the finite element procedure. Figure 7(b) shows plots of various terms in Equation (6) normalized with respect to the initial elastic modulus, E (see the appendix) versus the average axial strain. It can be seen that the term $(1 - D)C^{ep}$, which represents the modified elastoplastic RI response, is always positive. On the other hand, the plot of \bar{C} ($= C^{DSC}$), equation (6), shows that it becomes negative around the peak strain of about $\varepsilon = 0.018$, and becomes positive after the strain of about $\varepsilon = 0.07$, which denotes the end of the softening zone and the initiation of the residual condition. The term



(a)



(b)

Figure 7. Finite element results for one-dimensional tension test: (a) stress–strain behavior (b) tangent moduli vs. axial strain

$R(\sigma^c - \sigma^i)$, Figure 7(b), contributes to the negative values of \bar{C} in the softening zone. In the residual condition $dD \rightarrow 0$, hence, the third term, equation (6) tends to zero; however, since $0 \leq D_u \leq 1.0$ ($= 0.875$), the first two terms contribute to the small positive values of \bar{C} in the residual zone.

Mesh sensitivity

In order to show that the proposed DSC reduces the spurious mesh sensitivity, a problem involving a block of the concrete (properties given in the appendix) is subjected to uniform prescribed displacement loading, as shown in Figure 8. The loading involved 50 steps with each

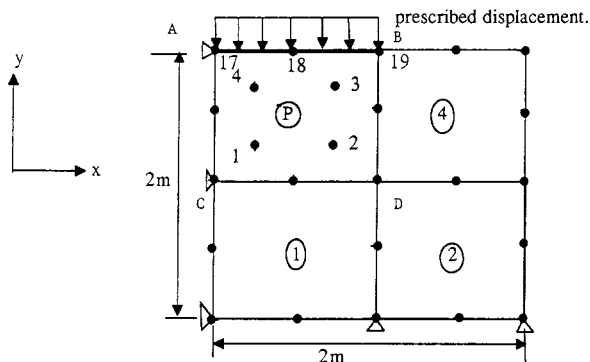


Figure 8. Mesh for concrete block

increment equal to 0.001 m. The right-hand side boundary is free to deform (Figure 8). The mesh is refined progressively in 4-, 16-, 64- and 256-eight-noded isoparametric elements with four-point Gauss integration. Plane strain idealization is adopted. The quarter of the block, e.g. ABCD, is considered to represent the tributary area for point P over which the nonlocal strains are computed using the following simple average:

$$\{\tilde{\varepsilon}\} = \frac{\sum_{i=1}^N \{\varepsilon_i\}}{N} \tag{24}$$

where ε_i is the local strain at the Gauss point i , and N is the number of Gauss points (in zone ABCD) for a given mesh. Then the average strain $\tilde{\varepsilon}$ is used to compute the following quantities required in equations (6), (8) and (17) for the elements belonging to the tributary area, e.g.

$$\tilde{\zeta}_D = \sum (d\tilde{E}_{ij}^p d\tilde{E}_{ij}^p)^{1/2} \tag{25a}$$

$$\{\tilde{\sigma}\} = [\bar{C}] \{d\tilde{\varepsilon}\} \tag{25b}$$

where $[\bar{C}]$ is evaluated using the average quantities. The RI state is characterized by using the δ_0 -model in the hierarchical single surface plasticity models,³¹ see Appendix.

Figures 9(a)–(c) show σ_y vs. ε_y , ε_v vs. ε_y , and $\sqrt{J_{2D}}$ vs. $\sqrt{I_{2D}}$, where σ_y and ε_y are stress and strain in the y -direction, respectively; ε_v the volumetric strain, J_{2D} and I_{2D} are the second invariants of the deviatoric stress and strain tensors, respectively. It can be seen that the finite element results involve essentially no spurious mesh sensitivity.

Laboratory verification

Figure 10(a) shows discretization of the cubical specimen tested under strain-controlled conditions by van Mier.³⁴ The test involved application of the prescribed displacement loading with increment = 0.05 mm over the top surface of the specimen with no confining stress (pressure); hence, the plane-strain idealization used here is considered to be satisfactory.

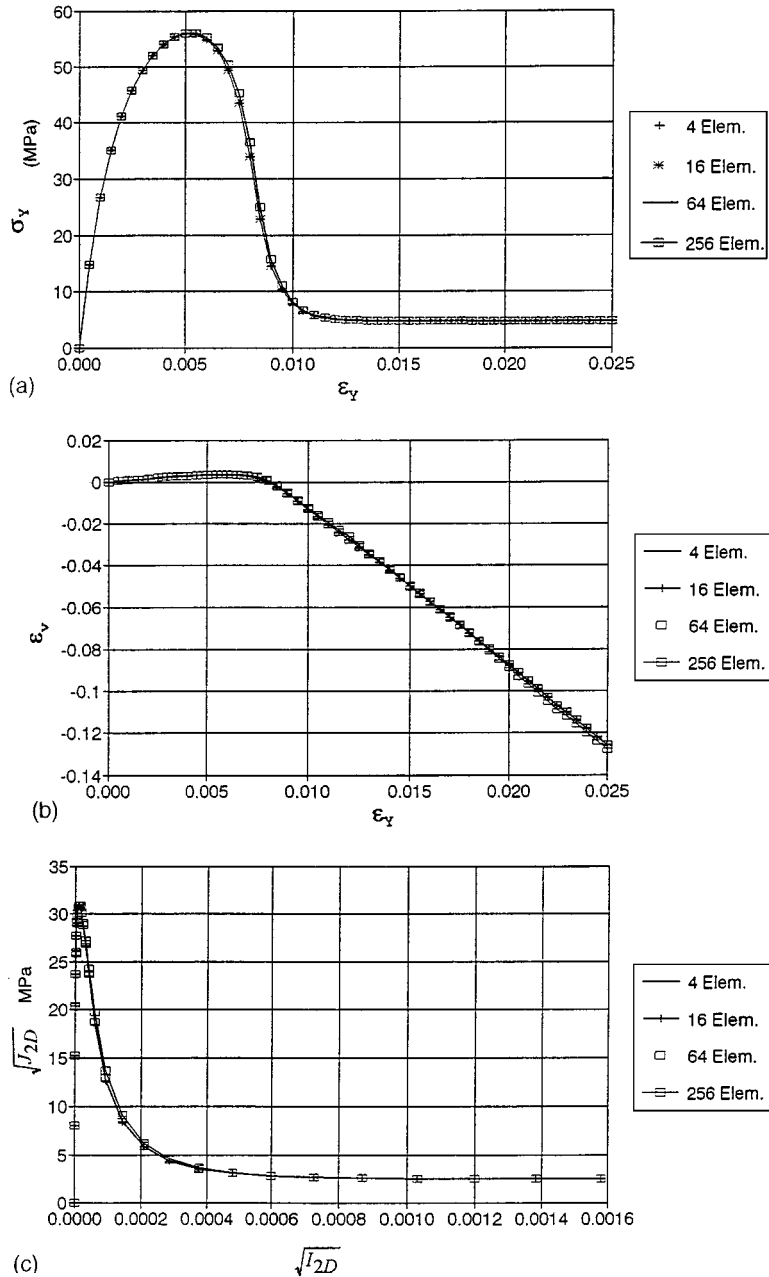


Figure 9. Typical results for Gauss point 3, element 3, Figure 8. (a) σ_y vs. ϵ_y (b) ϵ_v vs. ϵ_y ; (c) $\sqrt{J_{2D}}$ vs. $\sqrt{I_{2D}}$

As before, the test specimen was divided into 4-, 16-, 64- and 256-elements and the averaging procedure was used. The disturbance function, D , was calculated by using equation (7) based on the observed stress–strain behaviour in the test. Figures 10(b) and 10(c) show computed octahedral shear stress, τ_{oct} , vs. vertical strain ϵ_y , and volumetric strain, ϵ_v , vs. ϵ_y , in comparison

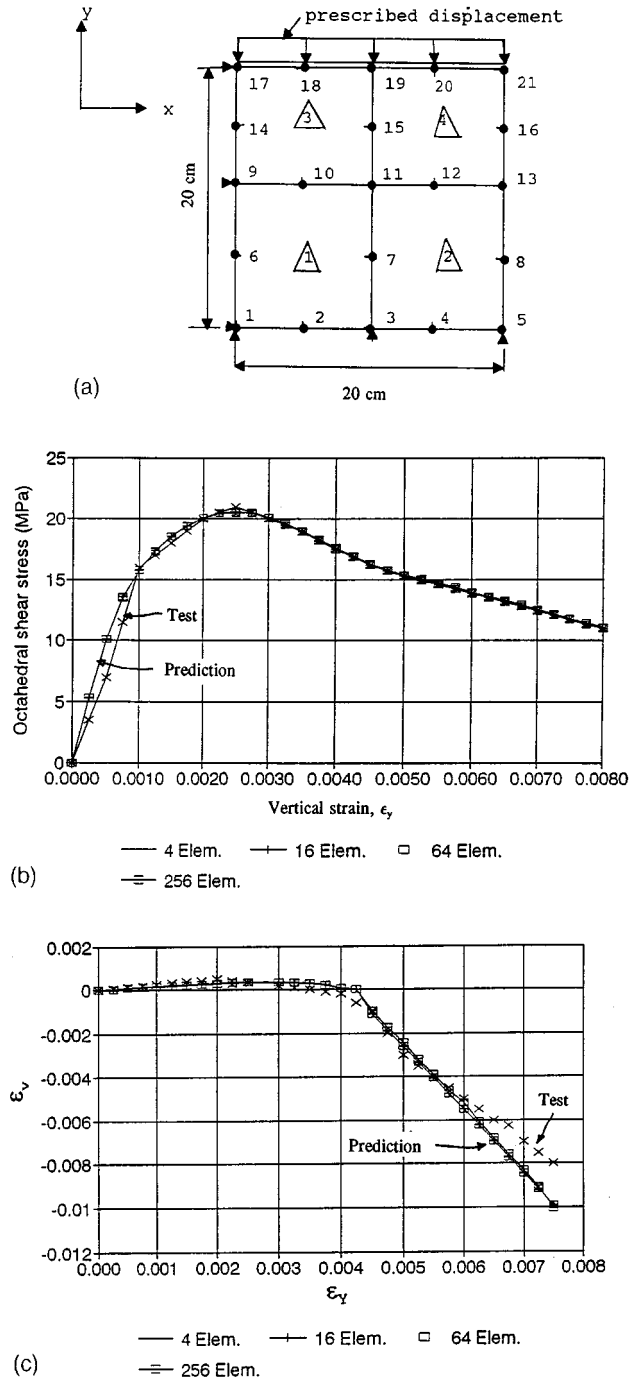


Figure 10. Comparisons of finite element prediction with laboratory test results for concrete: (a) finite element mesh; (b) τ_{oct} vs. ϵ_y ; (c) ϵ_v vs. ϵ_y

with the observations from the laboratory test. It can be seen that the results involve essentially no mesh sensitivity, and the computed results compare very well with the laboratory observation. These results can also be considered to indicate that the DSC procedure provides unique solutions.

Localization

Differences of opinion exist regarding the analysis of the existence and location of possible slip lines through the study of the acoustic tensor.^{36,5} For example, Zienkiewicz and Huang³⁷ have stated that ‘. . . acoustic tensor is a very unreliable indicator and that most of the reported difficulties result simply from using an incorrect finite element approximation in the solution of the plasticity problems involved’. The objective in the DSC is to develop a model that allows for localization, particularly with finer meshes, and also using adaptive mesh refinement; the latter is in progress.

To illustrate the computational and localization capabilities of the DSC, a number of problems have been solved. They include such problems as one-dimensional bar with imperfection, chip-substrate problem in electronic packaging, and development of wing cracks in concrete with an initial crack. Brief descriptions of the first two problems are given below.

Localization: one-dimensional bar problem with imperfection problem

The simple imperfect one-dimensional bar under tension (Figure 11(a)), is solved using the DSC. Other investigators, e.g. de Borst *et al.*⁵ have solved this problem to illustrate the

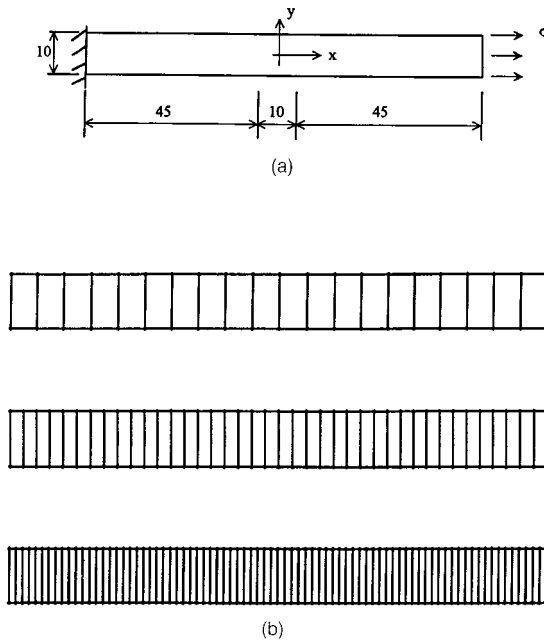


Figure 11. Tension bar with imperfection: (a) problem, (b) meshes

localization performance of their gradient-type regularization method. Figure 11(b) shows three meshes with 20, 40 and 80 eight-noded isoparametric elements. A part of the material properties used were the same as those by de Borst *et al.*⁵

Elastic modulus, $E = 20\,000$ MPa, Tensile strength, $\sigma_t = 2.0$ MPa

In order to utilize the isotropic hardening δ_0 -model,³¹ so as to represent the relative intact behaviour and to evaluate the parameters in the disturbance function, D , equation (8), the stress-strain curves in Reference 5 were used in an approximate manner. A small non-linearity with plasticity was considered, and the three curves for different values of l/L ($= 0.1, 0.05, 0.025$) were smoothed and extended to approach the residual stress states of about 1.0, 0.8 and 0.5 MPa, respectively. Here, l is the (arbitrarily chosen in Reference 5) small internal length, and L is the length of the bar. Then the parameters for the δ_0 -plasticity model involving continuous yielding and for D , were found as follows (see Appendix for definitions of parameters):

δ_0 -model.

Hardening:	$a_1 = 5.24$ $\eta_1 = 4.0 \times 10^{-10}$
Ultimate:	$\gamma = 1.1 \times 10^{-3}$ $\beta = 0.0$
State change:	$n = 2.1$

Disturbance

Case	l/L	A	Z	D_u
1	0.10	500	2.37	0.50
2	0.05	530	1.35	0.60
3	0.025	550	0.31	0.75

As was done by de Borst *et al.*,⁵ the middle zone of 10 mm was assigned reduced tensile strength by 10 per cent.

Computed results corresponding to $l/L = 0.05$, using the DSC for the three meshes are shown in Figure 12. Figure 12(a) shows satisfactory convergence in terms of total strain (ϵ) along the length of the bar. With the gradient model, the strain approaches the value of about 1.0×10^{-3} with 160 elements; the DSC model shows the similar value with 80 elements. The localization zone, w , predicted by the DSC is about 33 mm (Figure 12(a)). According to equation (47) in Reference 5, w is given by

$$w = 2\pi l \quad (26)$$

Hence, the value of l from the DSC is about 5.25 mm, which is comparable to $l = 5.00$ mm in Reference 5. It may be noted that the DSC does not involve l as a parameter in its formulation; hence, this comparison is presented mainly as an indirect validation. The computed results in terms of stress vs. displacement (Figure 12(b)), also show trends similar to those in Figure 3 (left) in Reference 5.

Figure 13 shows computed results for $l/L = 0.10, 0.05$ and 0.025 from the DSC for strain vs. length and stress vs. displacement for the 80-element mesh. Figure 13(a) shows consistent trends

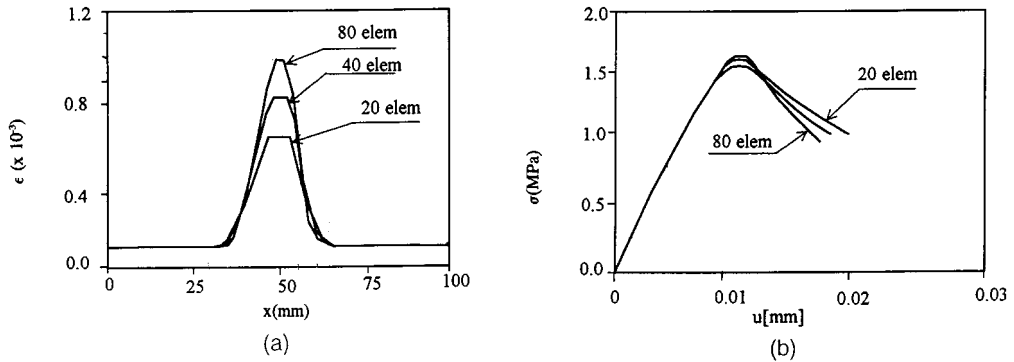


Figure 12. Computed results using DSC for $l/L = 0.05$: (a) total strain distribution along axis; (b) axial stress vs. axial displacement of right end of tension bar

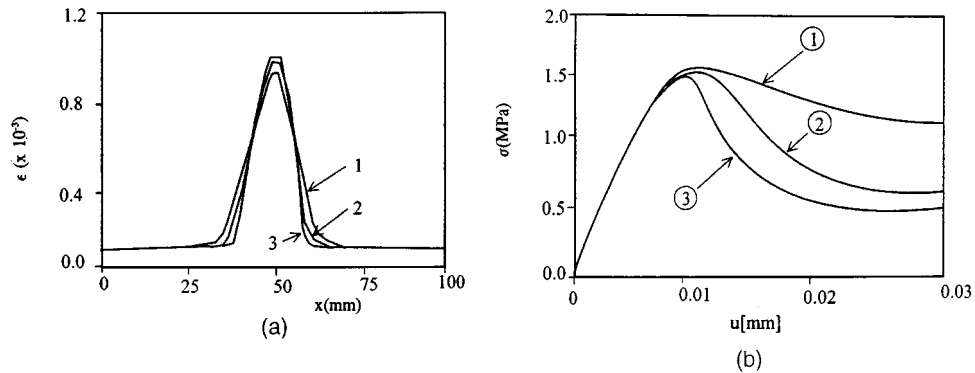


Figure 13. Computed results for 80-element mesh for three l/L ratios: (1) 0.10, (2) 0.05, (3) 0.025: (a) strain vs. length; (b) stress vs. displacement

in that the localization width, w , increases with l/L , indicating more brittle behaviour for smaller values of l . Use of equation (26) gives values of l for the three cases to be 3.2, 5.25, and 7.00 mm; these values are not the same as 2.5, 5.0 and 10.0 mm used in Reference 5. Figure 13(b) shows computed stress vs. displacement curves; here, although the overall magnitudes and trends are similar, the peak value of stress from the DSC and the gradient theory are somewhat different. Some of the reasons for these differences are stated below.

In the DSC, the plasticity δ_0 -model with the disturbance is used, while de Borst *et al.* used an elastoplastic (Drucker–Prager) model with the gradient enrichment. Also, some differences are introduced as the given curves were smoothed and the values of stresses and strains were adopted approximately by digitizing the curves. In the DSC, the plastic strains are developed from the beginning and, hence, there is non-zero disturbance before the peak stress; this may be a reason why the computed peak stresses are lower than those in de Borst *et al.*

Localization: chip–substrate problem

Figure 14(a) shows the finite element mesh for a leadless ceramic chip carrier joined to a printed wiring board by a Pb40-Sn60 solder about 0.203 mm thick; each element in the solder has size of 0.0476 mm × 0.0508 mm (Fig. 14(b)). This system was tested in the laboratory by Hall and Sherry³⁸ under a number of thermal cycles, (Figure 15), in which the temperature varied from − 25°C to 125°C.

The chip carrier and the printed wiring board were assumed to be elastic, while the DSC model with thermoviscoplastic properties was used for the solder.¹⁸ It may be noted that as viscosity is included, regularization is provided to a certain extent. Nonetheless, this problem illustrates the capability of the DSC in providing localization for a complex problem. Details of simulation and material properties are given by Basaran and Desai,¹⁹ a brief description of the latter is given below.

In the thermoviscoplastic model, quantities (ξ, ξ_D) are computed as trajectories of thermoviscoplastic strains, and various parameters, plastic and plastic hardening, are expressed based on laboratory tests on Pb–Sn solder as^{18,19}

$$p(\theta) = p_{300} \left(\frac{\theta}{300} \right)^\lambda \tag{27}$$

where p is the parameter, θ is the temperature, λ is the exponent and p_{300} is the value of p at 300 K. The viscoplastic strain rate is evaluated as

$$\{\dot{\epsilon}_n^{vp\theta}\} = \{\dot{\epsilon}_{n-1}^{vp\theta}\} + \left[\frac{\partial \dot{\epsilon}^{vp\theta}}{\partial \sigma} \right]_{n-1} \{d\sigma_n\} + \frac{\partial \dot{\epsilon}^{vp\theta}}{\partial \theta} d\theta_n \{I\} \tag{28}$$

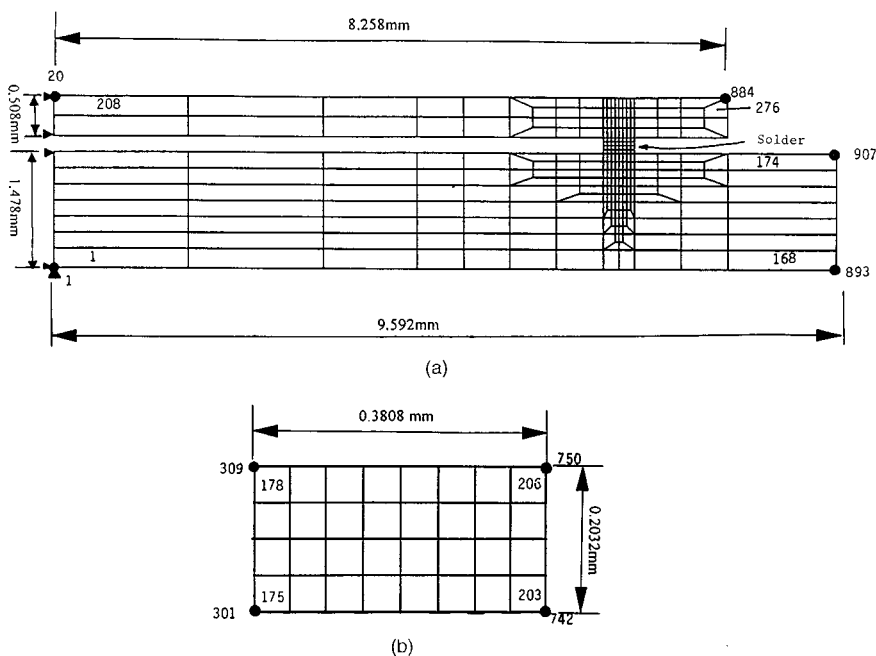


Figure 14. Finite element mesh for leadless ceramic chip carrier with Pb40-Sn60 solder joint: (a) mesh for chip–substrate problem; (b) magnified view of the finite element mesh for solder joint

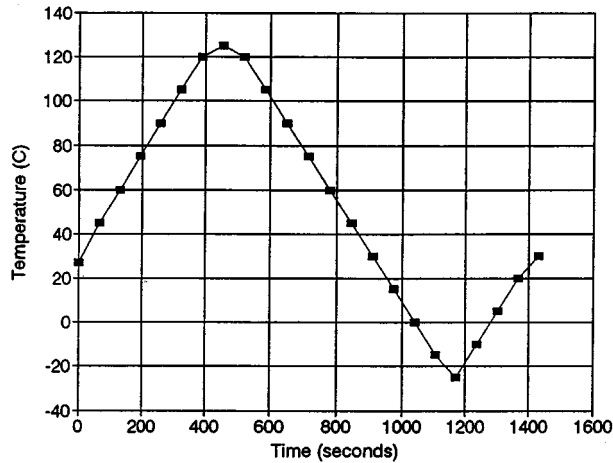


Figure 15. Time history of the temperature cycle; After Hall and Sherry³⁸

where $\{I\}$ is the unit vector, $vp\theta$ denotes thermoviscoplastic strain and the overdot denotes time rate.

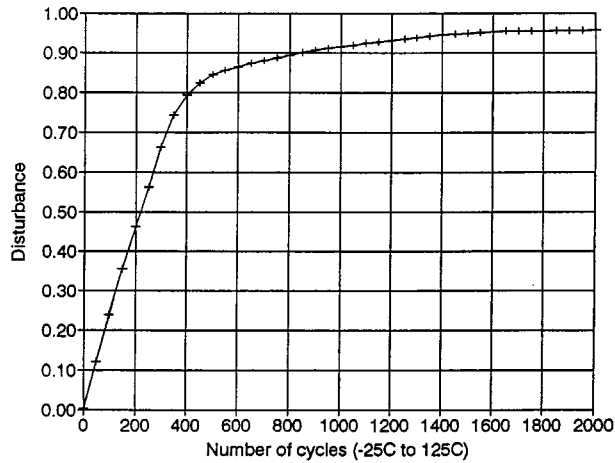
The finite element analysis was carried out for 2000 thermal cycles, and the results in terms of disturbance were plotted for different cycles N . Figure 16(a) shows computed growth of average disturbance with N over the elements in the solder, and Figure 16(b) shows the computed energy/cycle with N .

Plates 1(a), (b) and (c) show growth of disturbance, which is a function of plastic strains, for $N = 100, 300$ and 400 , respectively. For the configuration of chip–substrate system herein, the localization initiates at the upper right-hand corner in the solder. As the thermal loading (cycles) progresses, it grows in the upper third of the solder toward the upper left-hand corner; this is consistent with the laboratory and analysis reported previously.^{38,39} It was found that around $N = 350$, the major part, about 80–90 per cent, of the upper third of the solder, experiences critical disturbance D_c in the range 0.80–0.90; the solder can be considered to have failed in terms of its engineering service function under this condition. It can be seen in Figure 16 that at N equal to about 400, the rates of change of the disturbance and energy density per cycle show significant trend toward stabilization and saturation, indicating almost complete failure of the solder (Plate 1(c)). The value of N (between $N = 350$ and 400), at which critical localization leading to thermal fatigue failure occurs, is found to compare well with the value of the cycle at failure, $N_f = 346$, observed in the laboratory by Hall and Sherry.³⁸

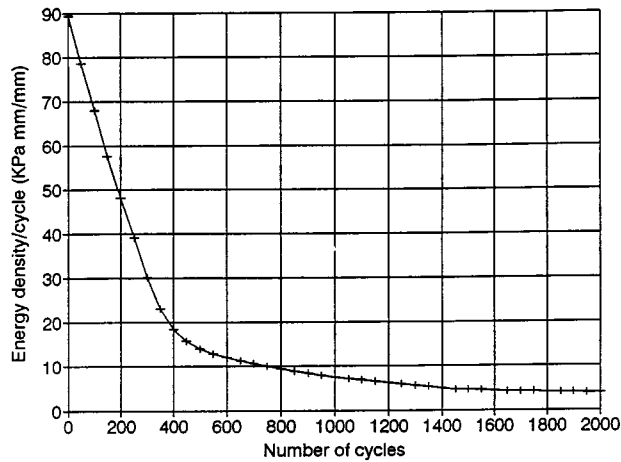
The above results indicate that the DSC provides satisfactory trends of growth and localization of the disturbance (strains).

CONCLUSIONS

The disturbed state concept allows for relative motions between the relative intact and fully adjusted parts of the material element. It is shown that localization limiter, size effect and microcrack interaction effects are included in the model. Furthermore, with the averaging of



(a)



(b)

Figure 16. Disturbance and energy density per temperature cycle in solder joint: (a) disturbance vs. temperature cycles; (b) energy density per temperature cycle vs. temperature cycles

strains over a tributary area, the DSC prevents loss of ellipticity. Provision of the averaging scheme and relative motions reduces significantly or eliminates for the problems considered herein the so-called spurious finite element mesh dependence. An analysis of the tangent stiffness matrix shows that the computer results provide convergent solutions. The DSC also provides a satisfactory comparison with the observed test results and can yield unique solutions. Also, it provides consistent and realistic trends of localization for a simple one-dimensional bar with imperfection, and complex chip-substrate problem under thermomechanical loading.

In view of the above findings, it is believed that the DSC provides a unified and holistic approach for modelling behaviour of materials undergoing microcracking and damage caused by

the self-adjustment of their internal microstructure. Furthermore, as the localization limiter, size effect and microcrack interaction effects are implicitly provided in the DSC model, it is not necessary to resort to enrichments such as Cosserat and gradient theories.

APPENDIX

Material parameters and model for relative intact state

The material parameters for the concrete were determined on the basis of multi-axial tests on cubical specimens reported by van Mier.³⁴ Their values are given below.

Relative intact

Elasticity:

$$\text{Elastic modulus, } E = 37\,000 \text{ MPa, Poisson's ratio, } \nu = 0.25$$

Plasticity:

Ultimate yield

$$\gamma = 0.0678, \quad \beta = 0.755$$

State change

$$n = 5.237$$

Hardening

$$a_1 = 4.61 \times 10^{-11}, \quad \eta_1 = 0.8262$$

Disturbance function

$$D_u = 0.875, \quad A = 688, \quad Z = 1.502$$

The elastic moduli, E and ν , were found based on the slopes of the unloading stress–strain curves. The plasticity parameters are related to the isotropic hardening plasticity HISS model³¹ in which the yield function F is given by

$$F = \bar{J}_{2D} - (\alpha \bar{J}_1^n + \gamma \bar{J}_1^2) (1 - \beta S_r)^{-0.5} = 0 \tag{29}$$

where S_r is the stress ratio $= (\sqrt{27}/2) J_{3D} J_{22}^{-1.5}$ is the third invariant of S_{ij} , n is the parameter related to the state at which the change in volumetric strain vanishes (e.g. transition from contraction to dilation), the overbar denotes non-dimensionalized quantity with respect to atmospheric pressure constant, p_a , γ and β are related to the ultimate envelope which is the locus of ultimate asymptotic stress state, and the hardening or growth function, α , is given by

$$\alpha = \frac{a_1}{\xi \eta_1} \tag{30}$$

in which a_1 and η_1 are hardening parameters, and $\xi = \int (d\epsilon_{ij}^p d\epsilon_{ij}^p)^{1/2}$. The disturbance parameters D_u , A and Z are found by using equations (7) and (8).

ACKNOWLEDGEMENTS

Parts of the research reported herein were supported by Grant Nos. DDM-9102177 and DDM-9313204 from Material Processing and Manufacturing, and Mechanics and Materials Programs, National Science Foundation, Washington, DC. Assistance and suggestions of Dr. H. B. Mühlhaus, particularly on the topics of ellipticity, size effects and localization, are gratefully acknowledged.

REFERENCES

1. H. L. Schreyer and Z. Chen, 'One-dimensional softening with localization', *J. Appl. Mech. ASME*, **53**, 791–797 (1986).
2. G. Pijaudier-Cabot and Z. P. Bazant, 'Nonlocal damage theory', *J. Eng. Mech. ASCE*, **113**, **10**, 1521–1533 (1987).
3. A. Needleman, 'Material rate dependence and mesh sensitivity in localization problems', *Comput. Methods Appl. Mech. Eng.*, **67**, 69–85 (1988).
4. Z. P. Bazant and L. Cedolin, in *Stability of Structures*, Oxford Univ. Press, New York, 1991.
5. R. de Borst, L. J. Sluys, H. B. Mühlhaus and J. Pamin, 'Fundamental issues in finite element analyses of localization of deformation', *Eng. Comput.*, **10**, 99–121 (1993).
6. J. R. Rice, 'Mathematical analysis in the mechanics of fracture', in H. Liebowitz (ed.), *Fracture, an Advanced Treatise*, Vol. 2, Academic Press, New York, 1968, pp. 191–250.
7. Z. P. Bazant and F. B. Lin, 'Non-local yield limit degradation', *Int. J. Numer. Meth. Engng.*, **26**, 1805–1823 (1988).
8. E. C. Aifantis, 'On the microstructural origin of certain inelastic models', *J. Eng. Mater. Technol.*, **106**, 326–334 (1984).
9. H. B. Mühlhaus and I. Vardoulakis, 'The thickness of shear bands in granular materials', *Geotechnique*, **37**, 271–283 (1987).
10. H. B. Mühlhaus and E. C. Aifantis, 'A variational principle for gradient plasticity', *Int. J. Solids Struct.*, **28**, 845–857 (1991).
11. R. de Borst and H. B. Mühlhaus, 'Gradient dependent plasticity: formulation and algorithmic aspects', *Int. J. Numer. Meth. Engng.*, **35**, 521–539 (1992).
12. A. C. Eringen, 'Theory of micropolar continuum', *Proc. 9th Midwestern Mech. Conf.*, Univ. of Wisconsin, Madison, Wisconsin, (1965), pp. 23–40.
13. E. Kroner, 'Elasticity theory of material with long-range cohesive forces', *Int. J. Solids Struct.*, **3**, 731–742 (1967).
14. C. S. Desai and Y. Ma, 'Modelling of joints and interfaces using the disturbed state concept', *Int. J. Numer. Anal. Meth. Geomech.*, **16**, 623–653 (1992).
15. C. S. Desai, 'Constitutive modelling using the disturbed state concept', in H. B. Mühlhaus (ed.), *Continuum Models for Materials with Microstructure*, Chap. 8, Wiley, U.K., 1995.
16. S. Armaleh and C. S. Desai, 'Modelling and testing of a cohesionless material using the disturbed state concept', *Int. J. Mech. Behavior Mater.*, **5**, 279–295 (1994).
17. D. R. Katti and C. S. Desai, 'Modelling and testing of cohesive soil using the disturbed state concept', *J. Eng. Mech. ASCE*, **121**, 648–658 (1995).
18. C. S. Desai, J. Chia, T. Kundu and J. L. Prince, 'Thermomechanical response of materials and interfaces in electronic packaging: Parts I and II', *J. Elect. Packaging ASME*, June 1997.
19. C. Basaran and C. S. Desai, 'Implementation of disturbed state concept for thermomechanical behavior of electronic packaging problems', *Report to NSF*, Dept. of Civil Engng. and Engng. Mechs., The University of Arizona, Tucson, Arizona, 1994.
20. C. S. Desai and J. Toth, 'Disturbed state constitutive modelling based on stress–strain and nondestructive behavior', *Int. J. Solids Struct.*, **33**, 1619–1650 (1996).
21. L. M. Kachanov, *Theory of Creep*, National Lending Library, Boston, Massachusetts, 1958.
22. L. M. Kachanov, *Introduction to Continuum Damage Mechanics*, Martinus Nijhoff Publishers, The Netherlands, 1986.
23. J. Lemaitre and J. L. Chaboche, *Mecaniques des Materiaux Solids*, Dunod-Bordes, Paris, 1985.
24. Z. P. Bazant, 'Nonlocal damage theory based on micromechanics of crack interactions', *J. Eng. Mech. ASCE*, **120**, **3**, 593–617 (1994).
25. D. Krajcinovic, 'Damage mechanics', *Mech. Mater.*, **8**, 117–197 (1987).
26. H. L. Schreyer, 'Analytical solutions for nonlinear strain-gradient softening and localization', *J. Appl. Mech. ASME Trans.*, **57**, 522–528 (1990).
27. H. B. Mühlhaus, R. de Borst, L. J. Sluys and J. Pamin, 'A thermodynamic theory for inhomogeneous damage evolution', *Proc. 9th Int. Conf. on Computer Methods and Advances in Geomech.*, Balkema, (1994), pp. 635–640.
28. P. Bak and K. Chen, 'Self-organized criticality', *Sci. Am.*, January 1991, 26–32 (1991).
29. G. Frantziskonis and C. S. Desai, 'Constitutive model with strain softening', *Int. J. Solids Struct.*, **23**, 751–767 (1987).

30. K. H. Roscoe, A. W. Schofield and C. P. Wroth, 'On yielding of soils', *Geotechnique*, **8**, 22–53 (1958).
31. C. S. Desai, S. Somasundaram and G. Frantziskonis, 'A hierarchical approach for constitutive modelling of geologic materials', *Int. J. Numer. Anal. Meth. Geomech.*, **10**, 225–257 (1986).
32. C. S. Desai, T. Kundu and G. Wang, 'Size effect on damage parameters for softening in simulated rock', *Int. J. Numer. Anal. Meth. Geomech.*, **14**, 509–517 (1990).
33. R. H. J. Peerlings, R. de Borst, N. A. M. Brekelmans and J. H. P. de Vree, 'Gradient enhanced damage for quasi-brittle materials', *Int. J. Numer. Meth. Engng.*, **39**, 3391–3403 (1996).
34. J. G. M. Van Mier, 'Strain softening of concrete under multiaxial loading conditions', *Ph.D. Dissertation*, Eindhoven Univ. of Tech., The Netherlands, 1984.
35. C. S. Desai and L. Woo, 'Damage model and implementation in nonlinear dynamic problems', *Int. J. Comput. Mech.*, **11**, 189–206 (1993).
36. R. Larsson, K. Runesson and N. S. Ottoson, 'Discontinuous displacement approximation for capturing plastic localization', *Int. J. Numer. Meth. Engng.*, **36**, 2087–2105 (1993).
37. O. C. Zienkiewicz and M. Huang, 'Localization problems in plasticity using finite elements with adaptive remeshing', *Int. J. Numer. Anal. Meth. Geomech.*, **19**, 127–148 (1995).
38. P. M. Hall and W. M. Sherry, 'Materials, structures and mechanics of solder-joints for surface-mount microelectronics technology', *Proc. 3rd Int. Conf. on Techniques de Connexion en Electronique*, Welding Society, Fellbach, Germany, February 1986.
39. D. R. Frear, H. Morgan, S. Burchett and J. Lau (eds.), *The Mechanics of Solder Alloy Interconnections*, van Nostrand Reinhold, New York, 1994.